Dispersion-Mediated Active-Layer Interfacial Regulation Using Halogenated Thioanisole Additives Achieves High-Efficiency Organic Solar Cells

Yanqi Shi,[a] Kun Li,[a] Yuan Yao,[a] Jingyue Guo,[a] Hui Chen,[b*] Yishi Wu,[a] Qing Liao,[a] Cunbin An,[a*] Hongbing Fu[a]

[a]*Beijing Key Laboratory for Optical Materials and Photonic Devices, Department of Chemistry, Capital Normal University, Beijing 100048, P. R. China.*

[b]*Institute of Chemistry, Henan Academy of Sciences, Zhengzhou 450002, China*

[*]Corresponding author.

E-mail addresses: ancunbin@cnu.edu.cn (C. An), chenhui@hnas.ac.cn (H. Chen)

Materials: All chemicals were purchased from commercial sources without further purification. PM6 and L8-BO were purchased from Solarmer Materials Inc. PEDOT:PSS (4083) was purchased from the CleviosTM. 4-FTA and 4-CTA were purchased from Energy Chemical. 4-BTA and 4-ITA were purchased from Adamas-beta®. All solvents were purchased from Sigma-Aldrich.

Device fabrication

Conventional OSC devices were fabricated with the architecture of ITO/PEDOT:PSS/active layer/PNDIT-F3N/Al. Indium tin oxide (ITO) glass substrates were sequentially subjected to ultrasonic cleaning in detergent solution, deionized water, acetone, and isopropanol for 15 min each, followed by drying under a nitrogen stream and subsequent plasma treatment for 10 min prior to use. PEDOT:PSS (aqueous dispersion) was spin-coated onto the ITO substrates at 5000 rpm for 30s and then thermally annealed at 150°C for 10 min. The donor PM6 and acceptor L8-BO were dissolved in chloroform at a donor-to-acceptor weight ratio of 1:1.2, with a total polymer concentration of 8 mg/mL. Additives 4-FTA and 4-CTA were incorporated at concentrations of 5 mg/mL, while 4-BTA and 4-ITA were incorporated at 10 mg/mL. The active-layer solutions were stirred at 55°C until complete dissolution, spin-coated onto the PEDOT:PSS layer, and subsequently thermally annealed at 100°C for 10 min. PNDIT-F3N was dissolved in methanol at a concentration of 1.4 mg/mL with the addition of 0.5 vol% acetic acid, and spin-coated onto the active layer at 4200 rpm for 20 s. Finally, an aluminum electrode (110 nm) was thermally evaporated under high vacuum (~5×10^{-4} Pa). The device active area was 0.037 cm^2, defined by a mask with an aperture area of 0.0256 cm^2.

Instruments and characterization

The absorption spectra of donor polymers and acceptors, both in solution and in solid thin films, were recorded using a HITACHI UH5700 UV–vis spectrophotometer. The current density–voltage (*J–V*) characteristics and power conversion efficiencies of the organic solar cells were measured under simulated 1 sun illumination (AM 1.5G, 100 mW cm^{-2}) using a XES-70S1 solar simulator (AAA grade, 70 mm × 70 mm beam size; SAN-EI ELECTRIC CO., Ltd.). The external quantum efficiency (EQE) tests were measured by using an integrated IPCE measurement system of QE-R3011 (Enli Technology Co. Ltd.).

Thermogravimetric analysis (TGA) measurements were carried out on TGA-2050

Thermogravimetry Analyze. The nanoscale morphology of the blend films was characterized using the Bruker AFM-DMFASTSCAN2-SYS operated in tapping mode.

The electron mobility was evaluated using the space-charge-limited current (SCLC) method with devices fabricated in the architecture of ITO/TIPD/active layer/PDINO/Al. Similarly, the hole mobility was measured using the SCLC method with devices fabricated in the configuration of ITO/PEDOT:PSS/active layer/Au. The carrier mobilities (μ_h or μ_e) were extracted by fitting the dark current characteristics to the single-carrier SCLC model, as described by the following equation:

$$J = \frac{9\varepsilon_0\varepsilon_r\mu V^2}{8L^3}$$

Where J is the current density, ε_0 is the vacuum permittivity, ε_r is the relative permittivity of the material, L is the thickness of the active layers and V is the effective voltage. The effective voltage is determined by subtracting the built-in voltage (V_{bi}) from the applied voltage (V_{appl}), $V=V_{appl}-V_{bi}$. The carrier mobility is calculated from the slope of the $J^{1/2}$-V characteristics.

Transient absorption (TA) measurements were conducted using a HARPIA-TA spectroscopy system (HARPIA, Light Conversion). A femtosecond laser source (PHAROS, Light Conversion) delivering pulses at a central wavelength of 1030 nm, with a pulse duration of 190 fs and a repetition rate of 100 kHz, served as the fundamental light source for the TA system. The laser output was split into two beams: the major portion was directed into an optical parametric amplifier (OPA, Light Conversion) to generate the pump pulses, while the remaining portion was used to produce the probe pulses in the form of a white-light supercontinuum (WLSc). The temporal delay between the pump and probe pulses was precisely controlled by a mechanical delay stage. All TA measurements were performed under ambient laboratory conditions at room temperature.

The GIWAXS samples were prepared on silicon substrates under the same conditions as those used for device fabrication. GIWAXS measurements were conducted at the 1W1A beamline of the Beijing Synchrotron Radiation Facility (BSRF). The crystalline coherence length (CCL) was determined using the Scherrer equation, where the d-spacing is given by $d=2\pi/q$ and the CCL is calculated as $CCL=2\pi K/FWHM$, with K being the shape factor (0.9 in this work) and FWHM representing the full width at half maximum of the diffraction peak.

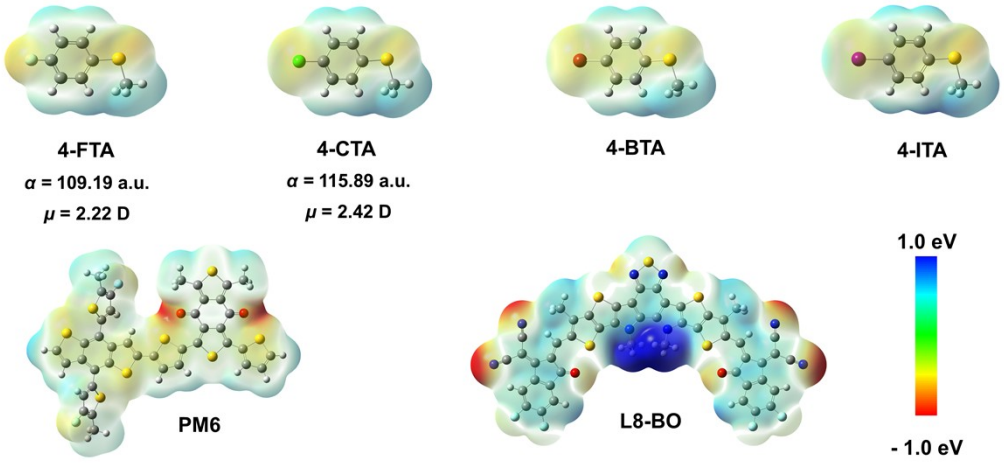

Fig. S1. The surface electrostatic potential distribution and average ESP values of PM6, L8-BO, 4-FTA, 4-CTA, 4-BTA, and 4-ITA.

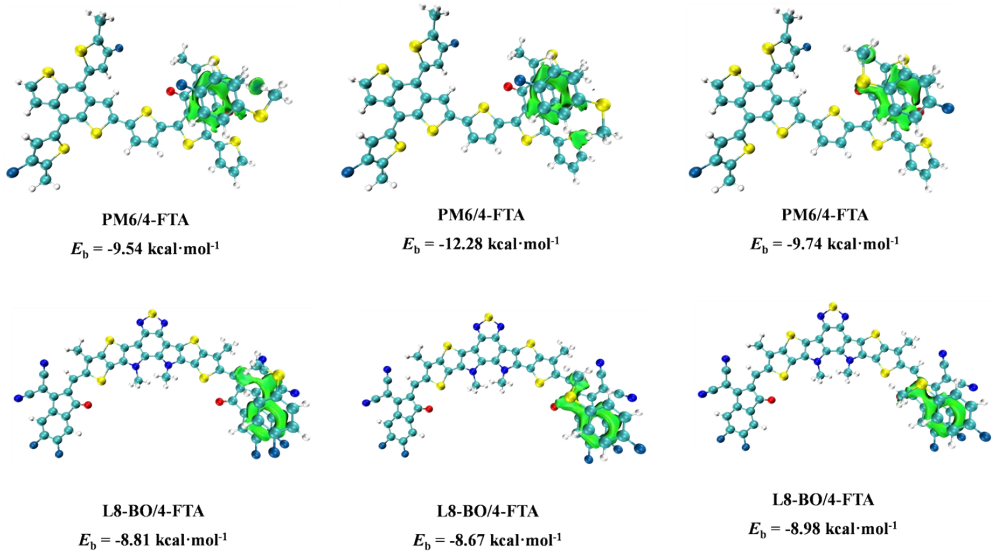

Fig. S2. The intermolecular interactions between the 4-FTA and PM6 and L8-BO were calculated at various sites.

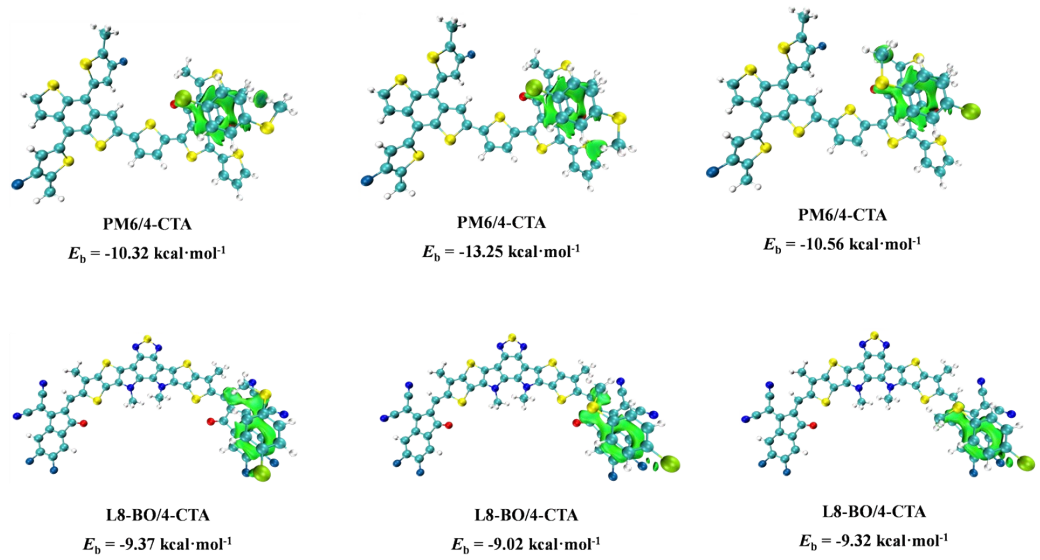

Fig. S3. The intermolecular interactions between the 4-CTA and PM6 and L8-BO were calculated at various sites.

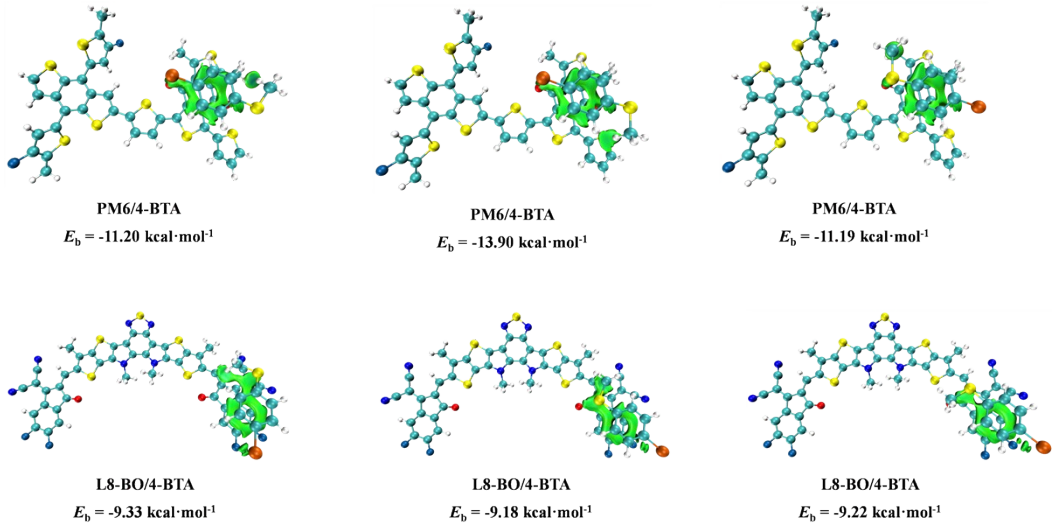

Fig. S4. The intermolecular interactions between the 4-BTA and PM6 and L8-BO were calculated at various sites.

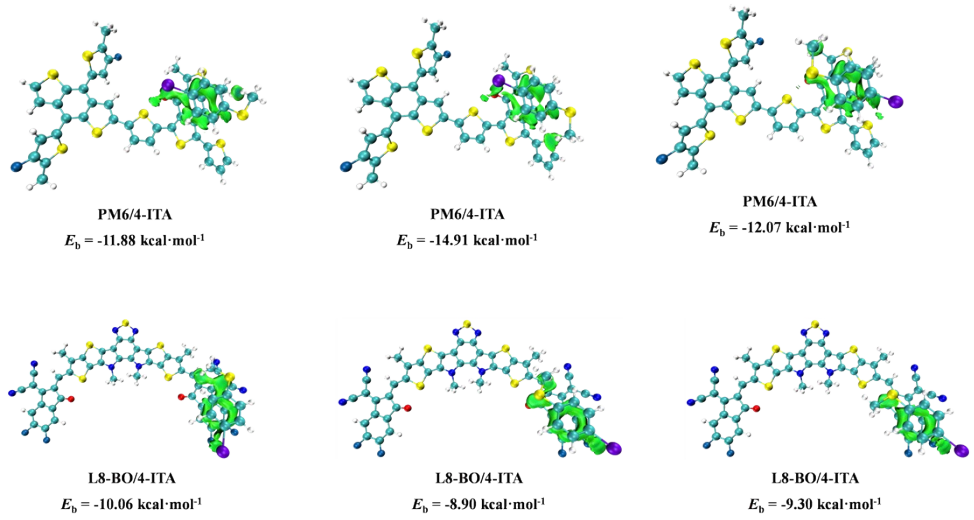

Fig. S5. The intermolecular interactions between the 4-ITA and PM6 and L8-BO were calculated at various sites.

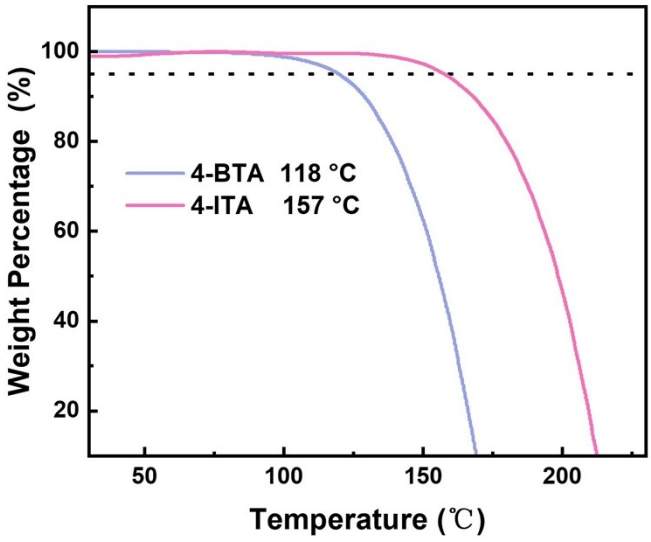

Fig. S6. TGA curves of 4-BTA and 4-ITA recorded at a heating rate of 5 °C min^{-1} under an inert atmosphere.

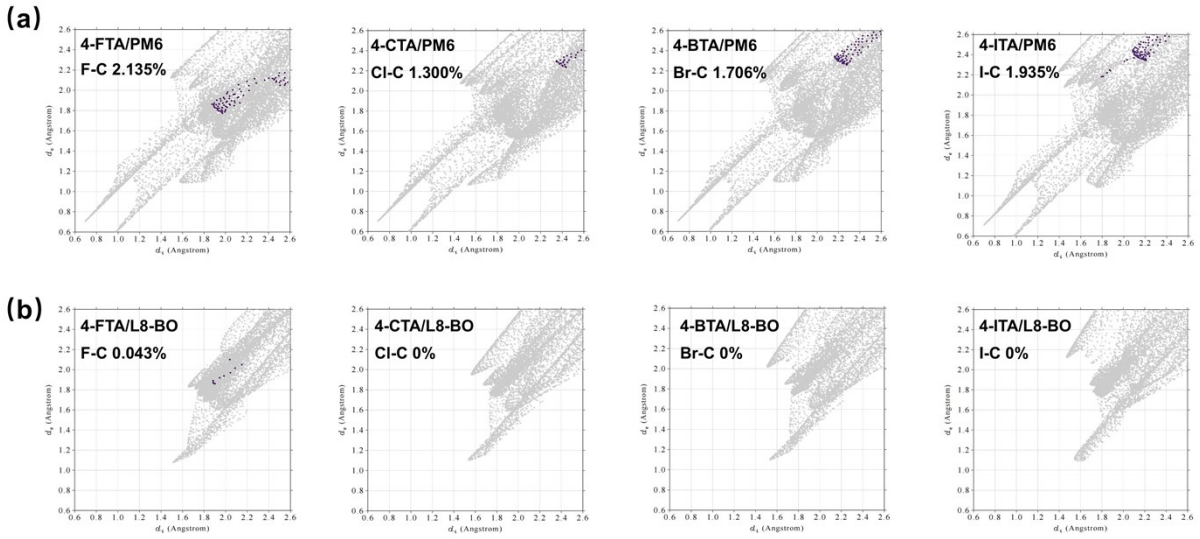

Fig. S7. RDG fingerprints showing X-C short-contact distributions for (a) PM6/additive and (b) L8-BO/additive interfaces.

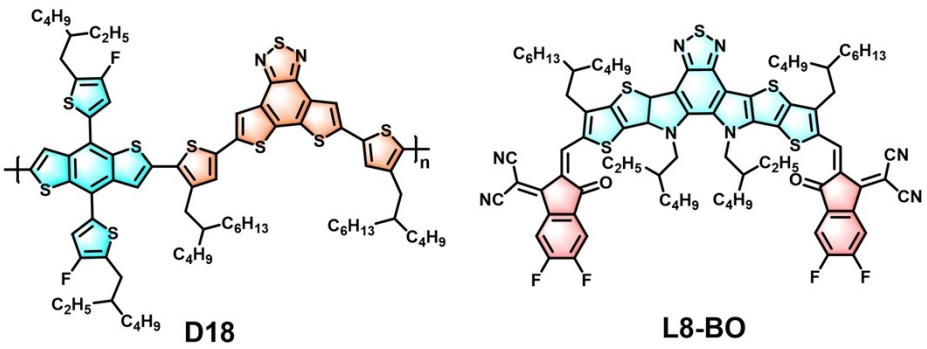

Fig. S8. Chemical structures of D18 and L8-BO.

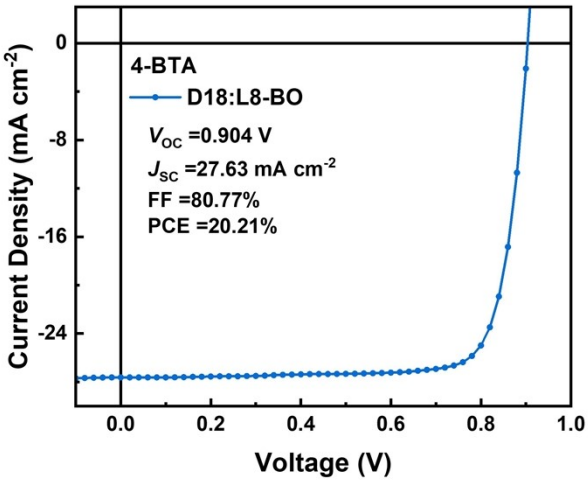

Fig. S9. *J-V* curve of D18:L8-BO device with additive under AM 1.5G (100 mW cm^{-2})

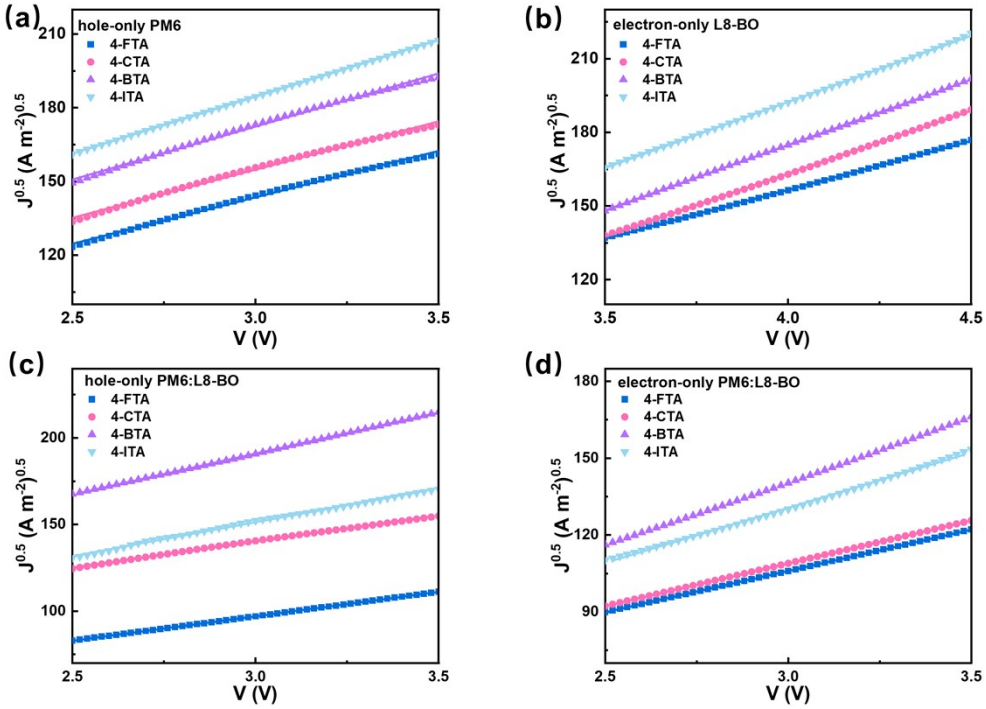

Fig. S10. (a) SCLC method for determining hole mobilities in PM6 neat films; (b) electron mobilities in L8-BO neat films with different additives; (c) hole mobilities in PM6:L8-BO blend films with different additives; (d) electron mobilities in PM6:L8-BO blend films with different additives.

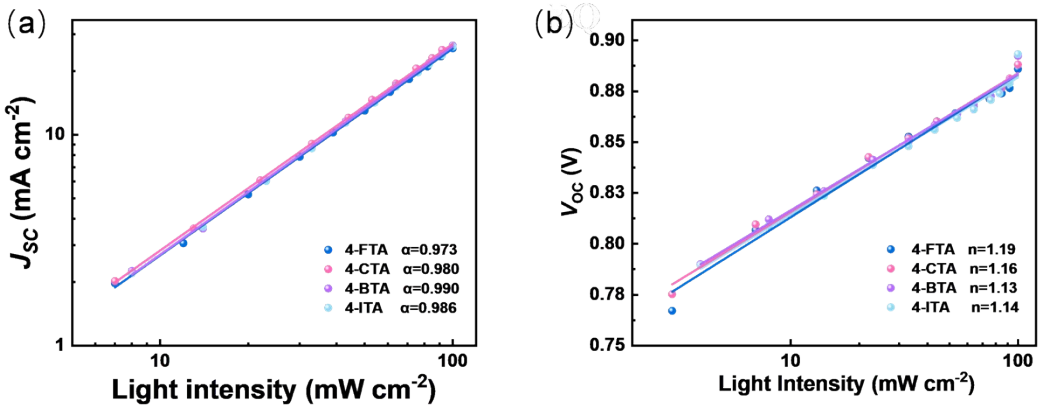

Fig. S11. Light-intensity dependence of (a) J_{SC} and (b) V_{OC} for the four PM6:L8-BO-based OSCs.

Table S1. Quadrupole moment distributions of the solid additives calculated using density functional theory (DFT).

Additive	Qxx (D·Å)	Qyy (D·Å)	Qzz (D·Å)
4-FTA	-2.38	6.04	-3.67
4-CTA	-1.05	5.64	-4.59
4-BTA	1.33	4.57	-5.90
4-ITA	3.13	4.42	-7.78

Table S2. Interaction energy components (total interaction energy E_{total}, electrostatic component ESP, and dispersion energy E_{disp}) calculated for PM6/additive complexes.

Blend	E_{total} [meV]	ESP [meV]	E_{disp} [meV]
PM6/4-FTA	-555.06	27.24	-833.80
PM6/4-CTA	-603.19	35.73	-925.58
PM6/4-BTA	-628.78	37.90	-951.29
PM6/4-ITA	-650.03	40.53	-976.82

Table S3. Interaction energy components (E_{total}, ESP, and E_{disp}) calculated for L8-BO/additive complexes.

Blend	E_{total} [meV]	ESP [meV]	E_{disp} [meV]
L8-BO/4-FTA	-441.59	255.88	-830.82
L8-BO/4-CTA	-451.96	253.33	-922.25
L8-BO/4-BTA	-455.85	252.04	-947.87
L8-BO/4-ITA	-457.15	242.92	-973.32

Table S4. Photovoltaic performance of the PM6:L8-BO based OSCs processed by different 4-FTA concentrations under AM 1.5G illumination at 100 mW cm^{-2}.

Concentration (mg/ml)	V_{OC} (V)	J_{SC} (mA/cm^2)	FF (%)	PCE (%)
3	0.891	25.40	73.06	16.45
5	0.889	26.18	73.31	17.07
10	0.849	25.41	75.89	16.36
15	0.705	24.01	62.33	10.54

Table S5. Photovoltaic performance of the PM6:L8-BO based OSCs processed by different 4-CTA concentrations under AM 1.5G illumination at 100 mW cm^{-2}.

Concentration (mg/ml)	V_{OC} (V)	J_{SC} (mA/cm^2)	FF (%)	PCE (%)
3	0.890	25.67	73.35	16.26
5	0.893	26.32	75.29	17.68
10	0.854	24.09	76.14	15.66
15	0.756	25.45	64.87	12.49

Table S6. Photovoltaic performance of the PM6:L8-BO based OSCs processed by different 4-BTA concentrations under AM 1.5G illumination at 100 mW cm^{-2}.

Concentration (mg/ml)	V_{OC} (V)	J_{SC} (mA/cm^2)	FF (%)	PCE (%)
3	0.893	24.14	73.01	15.74
5	0.901	25.16	75.19	17.05
10	0.894	26.84	80.68	19.32
15	0.851	23.52	76.22	15.25

Table S7. Photovoltaic performance of the PM6:L8-BO based OSCs processed by different 4-ITA concentrations under AM 1.5G illumination at 100 mW cm^{-2}.

Concentration (mg/ml)	V_{OC} (V)	J_{SC} (mA/cm^2)	FF (%)	PCE (%)
3	0.892	23.86	73.49	15.65
5	0.896	24.07	77.30	16.68
10	0.897	26.38	78.43	18.60
15	0.841	23.23	73.45	14.35

Table S8. GIWAXS characterization results of the blend films processed with different additives, including the q vector, d-spacing, and crystal coherence length (CCL) in the OOP direction, as well as the q vector and d-spacing in the IP direction.

Additive	IP		OOP			
treatment	q_{xy}(Å^{-1})	$d_{100\text{-spacing}}$ (Å)	q_z(Å^{-1})	$d_{010\text{-spacing}}$(Å)	FWHM(Å^{-1})	CCL(Å)
4-FTA	0.31	20.26	1.70	3.69	0.237	23.85
4-CTA	0.31	20.26	1.73	3.63	0.230	24.57
4-BTA	0.31	20.26	1.72	3.65	0.201	28.12

4-ITA	0.31	20.26	1.73	3.63	0.207	27.30